The Black Bug Myth: Selective Photodestruction of Pigmented Pathogens

David M. Harris, PhD,[1,2*] Steven L. Jacques, PhD,[3] and Richard Darveau, PhD[4]
[1]*Biomedical Consultants, Inc., Paradise, California 95969*
[2]*Department of Otolaryngology, University of Washington, Seattle, Washington 98195*
[3]*Departments of Biomedical Engineering and Dermatology, Oregon Health and Science University, Portland, Oregon 97239*
[4]*Department of Periodontics, University of Washington, Seattle, Washington 98195*

Background and Objective: It is commonly believed that pigmented pathogens are selectively targeted by dental lasers. To test this notion optical diffuse reflection spectroscopy (DRS) was used to obtain absorption spectra for the periodontal pathogens, *Porphyromonas gingivalis* (*Pg*) and *Prevotella intermedia* (*Pi*).
Materials and Methods: Spectra from 400 to 1,100 nm wavelengths of *Pg* colonies cultured with different concentrations of hemin were obtained to test the hypothesis that "visual pigmentation" predicts absorption of near-infrared (IR) dental laser energy. Ablation threshold at 1,064 nm [1] was measured for the pathogenic fungus, *Candida albicans* (*Ca*).
Results: The hypothesis was demonstrated to be true at 810 nm, it was false at 1,064 nm. Diode laser (810 nm) efficacy and "depth of kill" is dependent on hemin availability from 400 to about 900 nm. *Pg* and *Pi* absorption at 1,064 nm ($\mu_a = 7.7 \pm 2.6\,\mathrm{cm}^{-1}$) is independent of hemin availability but is determined by another unknown chromophore. *Ca* is non-pigmented but very sensitive to 1,064 nm irradiation.
Conclusions: The amount of visual pigmentation does not necessarily predict sensitivity to dental laser irradiation. Spectra in visible and near-IR wavelengths demonstrate a large difference in absorption between soft tissue and *Pg* or *Pi*. This difference represents a host/pathogen differential sensitivity to laser irradiation, the basis for selective photoantisepsis. Lasers Surg. Med.

Key words: dental laser; pulsed Nd:YAG; 810 nm diode; tissue spectroscopy; bacterial reduction; periodontal pathogens; *P. gingivalis* (*Pg*); *P. intermedia* (*Pi*); *C. albicans* (*Ca*)

INTRODUCTION

There is substantial evidence that dental laser treatment also destroys periodontal pathogenic bacteria [2–10]. The species most affected seem to be *Porphyromonas gingivalis* (*Pg*), *Prevotella intermedia* (*Pi*), and other dark-pigmented bacilli. From these observations there arose the idea that these pigmented pathogens are selectively targeted by near-IR dental lasers during a clinical procedure [11–13]. Since there appears to be no direct measurements to support this idea, only assumptions, we call it the "Black Bug Myth."

The primary endogenous pigment in *Pg* and *Pi* is thought to be concentrated hemin [14–17], although the possibility exists that other chromophores (light absorbing molecular species) account for *Pg* absorption in the near-IR. Newkirk et al. [18] reason that if hemin is the primary chromophore in these pathogens then the efficacy of selective destruction of pigmented pathogens by laser is dependent on hemin availability. It follows that there will be infected sites having limited access to blood and lymph circulation (privileged sites) where the pathogens will not be darkly pigmented and they will not absorb light. Consequently, they will be unaffected by laser irradiation and will remain as viable sites for recolonization.

The absorption coefficient, μ_a [cm^{-1}], is the parameter used to describe the effectiveness of light absorption by a material and depends on both the composition of the material and on the wavelength which is being absorbed. The set of measured values of μ_a for that material across a band of wavelengths is an absorption spectrum. The Black Bug Myth, restated as a testable hypothesis, predicts that the absorption coefficient of pigmented bacteria should be similar for visible light wavelengths as for the non-visible near-infrared wavelengths emitted by dental lasers. Comparison of absorption spectra in the visible and near infrared of pigmented and non-pigmented pathogens will provide empirical data to test the hypothesis.

Conflict of Interest Disclosures: All authors have completed and submitted the ICMJE Form for Disclosure of Potential Conflicts of Interest and none were reported.
Contract grant sponsor: NIH-NIDCR SBIR; Contract grant number: DE016180; Contract grant sponsor: NIH-NRSA; Contract grant number: DC008042.
*Correspondence to: David M. Harris, PhD, Biomedical Consultants, Inc., Paradise, 436 Green Oaks Drive, Paradise, CA 95969. E-mail: bmcinc@comcast.net
Accepted 25 May 2016
Published online in Wiley Online Library (wileyonlinelibrary.com).
DOI 10.1002/lsm.22545

MATERIALS AND METHODS

Bacteria Cultures

Methods for the incubation and irradiation of *Pg* cultured on Petri dishes are detailed previously [1,13]. Briefly, for ablation studies, colonies of a specific pathogen were grown from samples obtained from the American Type Culture Collection (ATCC). Stock cultures of *Pg* (ATCC #33277) and *Pi (*ATCC #25611) were maintained by anaerobic culture (85% N_2, 10% H_2, and 5% CO_2) at 37°C on LRBB agar (Brucella agar base supplemented with 5% laked rabbit blood, 5.0 μg/ml menadione, and 0.01% dithiothreitol, and 2.5 μg/ml hemin). *Candida albicans* (*Ca*) is a common fungal infection (candidiasis) of the gingival mucosa (Fig. 6) and implicated in periodontal disease [19–22]. *Ca* seeds (ATCC #10321) were streaked on LB agar (Lennox; Sigma, St. Louis) and incubated at 28°C for 2 days, until isolated colonies were approximately 1 mm in diameter. Nd:YAG laser irradiation studies were conducted to measure *Ca* ablation thresholds at 1,064 nm.

The Petri dish containing a culture was placed in the laser beam path and the irradiance in a single pulse that produced a just-detectable smoke plume or surface defect was measured. This defined the damage threshold for that sample under that set of conditions. The irradiance at the center of the Gaussian spot (twice the average fluence) produced a temperature increase to cause vaporization.

Darkly pigmented colonies of *Pg* and *Pi* were grown in a broth suspension for spectroscopy. The medium included tryptic soy broth 30 gm/L, yeast extract 5 gm/L, menadione 1.0 mg/L, and hemin 10 μg/ml. Colonies of *Pg* were also incubated with a variable hemin concentration (0.5, 1, 2, 5, 10, and 15 μg/ml) in order to test the Black Bug hypothesis. Filter-sterilized hemin was added to the autoclaved medium, and 10 ml volumes at each concentration of hemin were inoculated with bacteria and grown overnight. Then, 100 ml bottles were inoculated with the 10 ml overnight cultures and grown for 15 1/2 hours. The 100 ml cultures were centrifuged. The pellet was resuspended in 1.0 ml of PBS and a small (10 μl) sample of this resuspension was further diluted 1:10 by addition of PBS (90 μl) for use in measuring the turbidity (optical density, O.D.) to determine cell density. The remaining 990-μl suspension was recentrifuged. The pellet was resuspended in a ~1-ml volume of PBS, whose volume was adjusted such that the final concentration of cells was 10^{10} cells/ml.

The method of measuring bacteria absorption was to measure the reflectance from a scattering solution then add bacteria and measure the change in reflectance. The scattering solution consisted of 500-nm-diameter polystyrene microspheres in water at a 10% volume fraction.

A 0.6-ml aliquot of each washed bacterial suspension was mixed with 1 ml of scattering solution. Hence, the final concentration of bacteria in the test solution was (0.6/1.6 ml) (10^{10} cells/ml) $= 3.8 \times 10^9$ cells/ml, and the final microsphere volume fraction was 6.25%.

Collection of Spectra

The absorption spectra of *Pg* and *Pi* were measured by adding the bacterial suspension to the scattering solution and observing the change in diffuse reflectance (Fig. 3). The raw reflectance spectra are calibrated relative to the change of simply adding clear buffer (no additional absorption) and the change from adding a known amount of absorber, India ink (see Appendix).

With the room lights off white light from a halogen lamp (HL-200, Ocean Optics 0, Dunedin, FL) was delivered through an optical fiber bundle and lens to illuminate the surface of the test solution (about 1-cm diameter spot). The diffuse light in the solution did not extend to the edge of the well, so edge effects were avoided. A 1-mm diameter optical fiber was used to sample the diffuse reflection. It was positioned to view the sample from a 45° angle to reduce the specular reflectance from the solution surface (i.e., surface glare) (Fig. 1). The collection fiber led to a VIS-IR spectrometer (QE65000, Ocean Optics, Dunedin, FL). Spectra were acquired over the 400–1,100 nm wavelength range. The raw reflectance spectra were normalized relative to controls and then converted to absorption spectra for the bacteria. The calculations are detailed in the Appendix.

RESULTS

Damage Thresholds of Periodontopathogens

It was previously reported that the damage threshold for *Pg* in culture was 58 J/cm^2 for the pulsed Nd:YAG laser at 1,064 nm (100 μsec pulse) and 96 J/cm^2 for 810 nm diode laser (100 msec pulse) [1,13]. The average ($N = 5$) damage threshold for *Ca* in culture with a pulsed NdYAG (1,064 nm, 100 μsec pulse) was measured as 4.9 J/cm^2. For thermal damage experiments *Pg* colonies were grown in 2.5 μg/ml hemin.

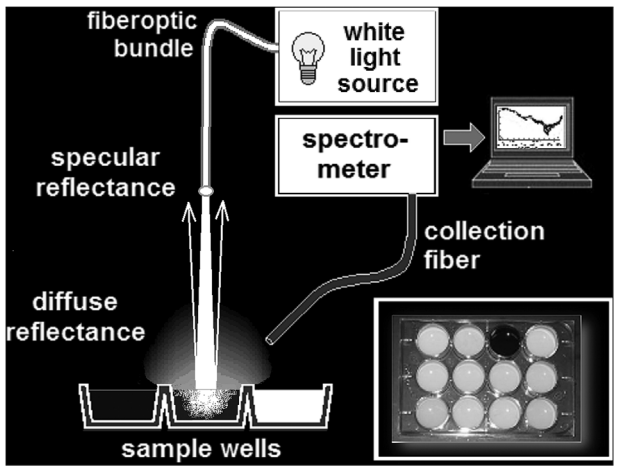

Fig. 1. Diffuse reflection spectroscopy of bacteria suspended in water and microspheres. The 45° angle of the collection fiber avoids surface reflectance. The portion of white light absorbed by the bacteria is absent from the diffuse reflectance that is sampled by the collection fiber. Inset: test solutions in a 12-well culture dish. Note the well with black ink, used for calibration.

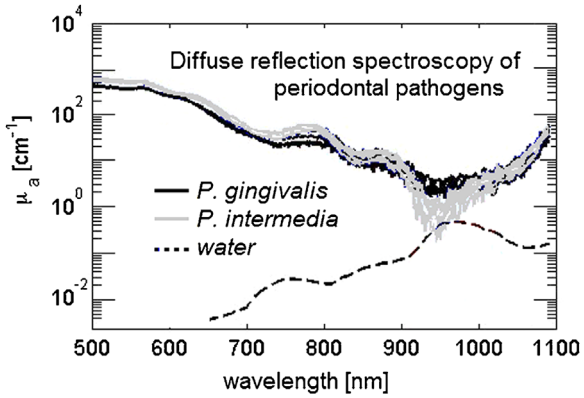

Fig. 2. Absorption spectra of *Pg* (black) and *Pi* (gray). The absorption of pure water (dotted line) is also shown, which closely matches the absorption of the bacteria near 960 nm. The bacterial absorption is about $10\,\mathrm{cm}^{-1}$ at 1,064 nm, while the background water absorption is $0.1\,\mathrm{cm}^{-1}$, a 100-fold greater absorption by the bacteria.

Absorption Spectra of Periodontopathogens

Presented in Figure 2 are absorption spectra of darkly pigmented *Pg* and *Pi* cultured *in vitro*. Both species of bacteria have similar optical properties showing higher absorption than the surrounding tissues across the visible and near-IR spectrum. The absorption of pure water closely matches the absorption of the bacteria near 960 nm. There is a large difference in absorption between the pathogens and water in the host tissue in the visible, very near IR (<900 nm) and in the vicinity of 1,064 nm. At 1,064 nm there is a 100-fold difference in absorption between the pathogens and the host tissues (water is the primary chromophore in soft tissue at this wavelength).

Absorption Spectra of *Pg* Cultured With a Hemin Gradient

Figure 3 (inset) shows vials containing *Pg* colonies that were incubated in a gradient of hemin concentrations. It is clear that hemin concentration determines the amount of visual pigmentation. Leung et al. [17] observed a similar relationship between optical density (absorbance) at 550 nm and hemoglobin binding in *Pi*. The absorption spectra acquired from these samples show quantitatively this relationship between the absorption coefficient, μ_a, and hemin concentration in the visible and very near IR portion of the spectrum (400–900 nm). At wavelengths longer than about 940 nm there appears to be little correlation.

Figure 4 plots the absorption coefficient of *Pg* at 633 nm (the visible red wavelength of a HeNe laser), 810 nm (the near-IR wavelength of the diode laser used in ablation experiments [1,13] and 1,064 nm (the near-IR wavelength of the pulsed Nd:YAG laser) as a function of the hemin concentration in the original culture medium. Each data set is fit with a linear regression. The optical absorption of *Pg* at 633 nm shows a strong dependence on the concentration of hemin ($\mu_a = 17\,\mathrm{cm}^{-1}$ per 1 μg/ml of hemin. The relation is also dependent on hemin, although not as dramatic, at 810 nm ($\mu_a = 1.2\,\mathrm{cm}^{-1}$ per 1 μg/ml of hemin. However, the absorption at 1,064 nm is not dependent on hemin, and is roughly constant at $\mu_a = 7.7 \pm 2.6\,\mathrm{cm}^{-1}$ for all concentrations.

DISCUSSION

Absorption Coefficients for *Pg* and *Ca* Are Derived From Damage Threshold Data

Damage threshold data at a specific wavelength are converted to absorption coefficients at that wavelength in order to relate those data to the optically measured absorption spectra in Figure 3. This is a key relationship that bridges the gap between physics (tissue optics) and clinical outcomes (tissue damage).

Tissue damage threshold is a function of both time and temperature such that shorter duration exposures need to achieve higher temperatures in order to cause tissue damage. Thermal damage to a *Pg* colony can be modeled approximately by the kinetics of soft tissue denaturation, which typically involves disruption of molecular bonds equivalent to ~15 hydrogen bonds [23]. This equals a molar enthalpy $(\Delta H \approx 19 \times 10^3\,\mathrm{J/mol} \times 15 = 2.9 \times 10^5\,\mathrm{J/mole})$ for irreversible denaturation. The molar entropy is expected to be $\Delta S = 31.47 \times 10^{-4}\Delta H\ -327.5 = 585.1\,\mathrm{J/(mol\,K)}$. The exposure time, t (s), to achieve denaturation is $t = 1/k$, where $k = (k_B T/h)\exp(\Delta S/R\ -\Delta H/(\mathrm{RT}))$ (s^{-1}), and T is temperature (Kelvin), k_B is the Boltzmann constant, h is Planck's constant, and R is the gas constant. Plotting t *versus* T/273.15 (Celsius) yields Figure 5. With this model, an 111°C exposure temperature for a 100 μsec exposure time or an 84°C temperature for 100 msec will achieve thermal damage.

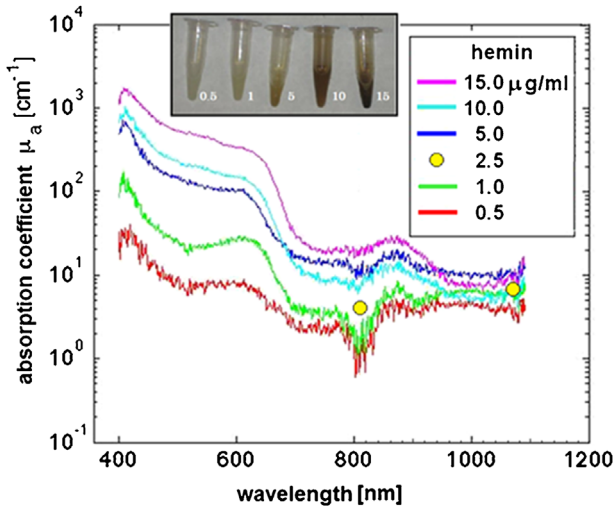

Fig. 3. Absorption coefficients (μ_a) of *Pg* suspended in microspheres acquired from 400 to 1,100 m with diffuse reflection spectroscopy. Spectra were obtained from colonies incubated in a gradient of hemin concentrations. Also plotted are the absorption coefficients for *Pg* (yellow circles) derived from thermal damage measurements. Inset: Vials containing *Pg* samples indicate that the intensity of visual pigmentation varies with hemin concentration. Leung et al. [17] observed a similar relationship between optical density (absorbance) at 550 nm and hemoglobin binding in *Pi*.

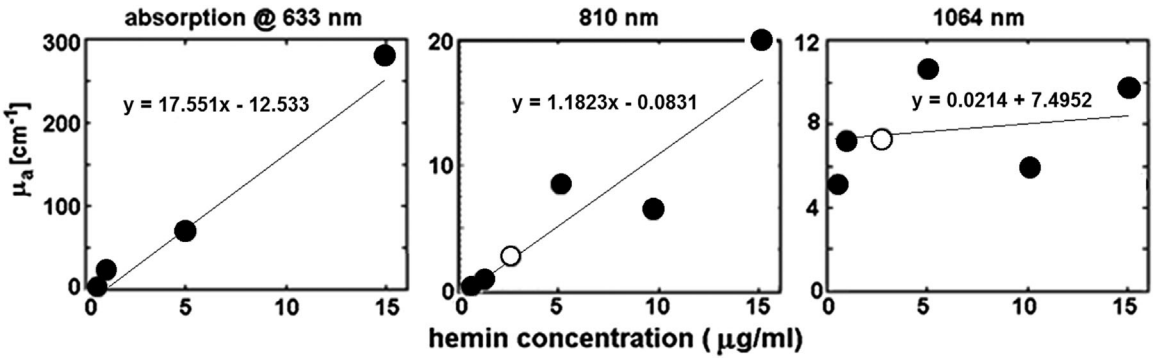

Fig. 4. Values of the absorption coefficient (μ_a) of *Pg* cultured in different concentrations of hemin at three different wavelengths: 633 nm (visible), 810 nm (diode laser), and 1,064 nm (Nd:YAG laser). There is a linear relationship between hemin concentration and *Pg* absorption at 633 nm and 810 nm but not at 1,064 nm. Filled circles are values of ìa derived from spectroscopy. Open circles are absorption coefficients derived from thermal damage measurements.

At room temperature (24°C) the threshold radiant exposure (H_{th}) causing damage for *Pg* in culture is 58 J/cm^2 for the pulsed Nd:YAG at 1,064 nm (100 μsec pulse), 96 J/cm^2 for 810 nm diode laser (100 msec pulse) and for *Ca* in culture the H_{th} is 5 J/cm^2 (1,064 nm, 100 μsec pulse). One can estimate absorption coefficients from these H_{th} values.

The absorption coefficient of *Pg* in a solution is estimated by the energy required to raise the temperature of pure water by ΔT and the energy deposition required to raise a solution of water + *Pg* by the same ΔT. The equation computes the minimum concentration of absorbing pigment, expressed as the minimum optical absorption coefficient, μ_a, that would allow a single laser pulse to thermally damage bacteria. In this case ΔT is the change in temperature from ambient ($T_i = 24$°C) to thermal damage threshold (T_f):

$$\mu_a = \left(T_f - T_i\right) \times \rho \times \mathrm{C}_p / H_{\text{th}},$$

where ρ = density [g/cm^3], C_p = specific heat (4.3 [J/gK]), H = radiant exposure to achieve the temperature jump (J/cm^2). It is assumed that the bacteria have a density that is the same as water (1 g/cc) and a heat capacity that is the same as water (4.18 kJ/g°C), calculated as follows:

$$\text{At } 810\text{ nm } \mu_a P_g = \left([84-24]^\circ\mathrm{C} \times 4.18\,\mathrm{J/cm^3}\,/1^\circ\mathrm{C}\right)/ 96\,\mathrm{J/cm^2} = 2.6\ \mathrm{cm^{-1}}$$

$$\text{At } 1,064\text{ nm } \mu_a P_g = ([111-24] \times 4.18)/58 = 6.3\ \mathrm{cm^{-1}}$$

$$\text{At } 1,064\text{ nm } \mu_a C_a = ([111-24] \times 4.18)/5 = 73\,\mathrm{cm^{-1}}$$

The absorption coefficient of *Pg* at 1,064 nm derived from damage threshold measurements, $\mu_{aPg} = 6.3\,\mathrm{cm^{-1}}$, compares well with $\mu_{aPg} = 7.7\,\mathrm{cm^{-1}}$ from the spectroscopy data. Also, the value of $\mu_{aPg} = 2.6\,\mathrm{cm^{-1}}$ at 810 nm for *Pg* colonies grown in 2.5 μg/ml hemin falls within the 1.2–10.0 cm^{-1} range of μ_{aPg} with hemin concentrations of 1–5 μg/ml at 810 nm as measured with spectroscopy. Yellow circles in Figure 3 and open circles in Figure 4 represent values for μ_{aPg} derived from damage thresholds. The two very different methods that were used to derive pathogen absorption coefficients yielded quite similar results that provide verification of the methodologies.

The Black Bug Myth

The black bug hypothesis is true at 810 nm but falsified at 1,064 nm. The data show that hemin availability does correlate with the visual pigmentation of *Pg*. And, the absorption of 810 nm wavelength by *Pg* is also dependent on hemin concentration. However, *Pg* absorption at 1,064 nm is not related to hemin concentration but is mediated by an unknown chromophore. Also, absence of dark pigment does not necessarily mean absence of absorption in the near-IR. *C. albicans* is white to milky white in appearance (Fig. 6), yet has a very high absorption coefficient at 1,064 nm of 73 cm^{-1}.

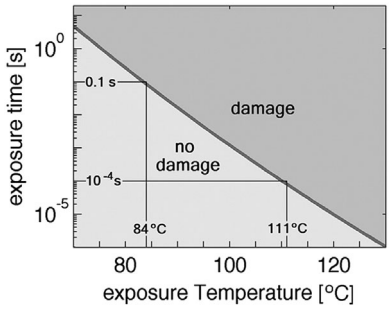

Fig. 5. The expected exposure time and exposure temperature required to achieve thermal damage in a *Pg* colony [23]. Short duration exposures need to achieve higher temperatures at the target to cause thermal damage.

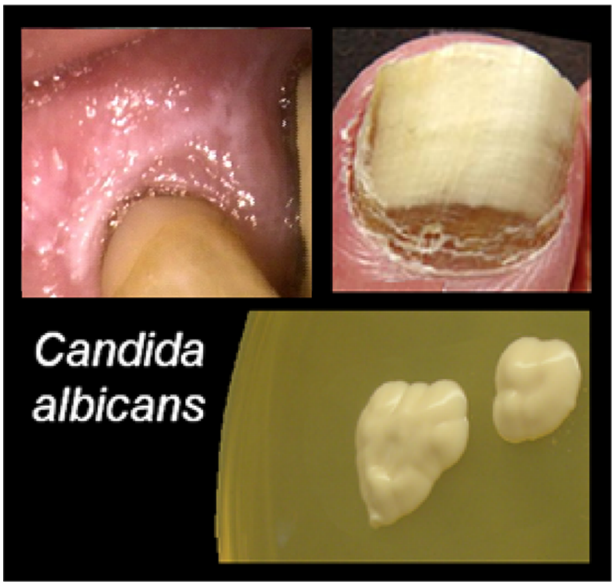

Fig. 6. UL: Oral thrush (*Candida albicans*, *Ca*). UR: Great toe nail infected with *Ca*. Bottom: *Ca* in culture. *Ca* is a non-pigmented fungal pathogen yet it is damaged at a low threshold in culture (5 J/cm^2 @ 1,064 nm) and responds rapidly to photo-antisepsis through the nail plate using a pulsed Nd:YAG laser [24]. Photo of oral thrush provided by Dr. Todd McCracken, DDS.

Newkirk et al. [18] question whether "selective black pigmented bacterial kill" occurs *in situ*. Although these pathogens may be pigmented in culture, there is no evidence that they are pigmented in the periodontal pocket as well. This argument applies to VIS-IR wavelengths less than 900 nm. But it appears to be irrelevant at 1,064 nm.

The significance of these observations is that the amount of visual pigmentation, or lack of pigmentation does not predict sensitivity to non-visible wavelengths longer than about 900 nm. Furthermore, these pathogens can be heated by a pulsed Nd:YAG laser regardless of their access to hemin during culture. This suggests that *Pg* and *Pi in vivo* in the periodontal tissues can be targeted for destruction by the pulsed Nd:YAG laser whether or not the bacteria have access to hemoglobin.

Selective Photoantisepsis

An important result is quantification of the differential sensitivity between the pathogens (*Pg*, *Pi*, and *Ca*) and the surrounding soft tissues. The implication is that normal tissues can be spared while these pathogens are targeted and destroyed at a depth following surface irradiation with a laser. The data indicate that both 810 nm diode and Nd:YAG lasers are capable of selective photoantisepsis due to differential absorption between the host tissue and the pathogens. A unique aspect of laser irradiation is that it affects extracellular and intracellular pathogens equally [25] (Fig. 7) and can access other privileged sites such as calculus and dentinal tubules. Photoantisepsis has no expected negative systemic side-effects, or interactions with other modes of therapy.

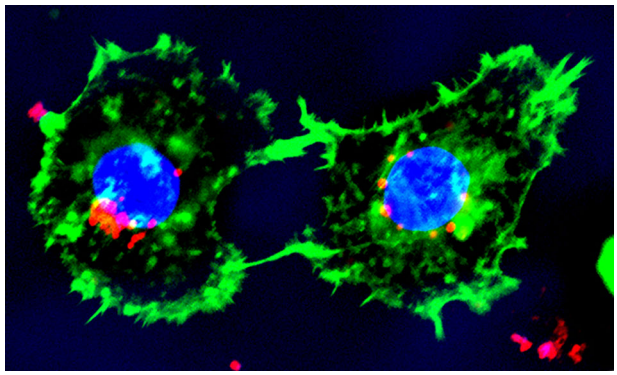

Fig. 7. "Immunologic sanctuary." Immuno-histofluorescent confocal microscopy of *Pg* (red) residing within the cytoplasm of gingival epithelial cells (green). The cell nucleus is stained blue. *Pg* and other bacteria can enter epithelial cells wherein they can replicate and influence cell metabolism [15,32]. Intracellular bacteria evade host immune effectors and chemical antibiotics commonly used to treat infection. However, at wavelengths where cells are optically transparent this evasion tactic does not avoid destruction by laser irradiation [1,25]. Invasion assay provided by Stephan R Coats, PhD, University of Washington.

Selective photoantisepsis is achieved during laser periodontal surgery, but inadvertently as a consequence of the surgical procedure. A proactive application of selective photoantisepsis requires a better understanding of how deep the effect extends, the sensitivity of the vast variety of periodontal pathogens to specific wavelengths and the appropriate laser parameter set to achieve maximum efficacy. A computational model of the infected periodontium has been developed to address these questions [29–32].

ACKNOWLEDGMENTS

The authors thank Pamela Braham, Dr. Sam Lewis, Ali Divan, and Jeremy Ault for preparation of *in vitro* pathogen samples and Lou Reinisch and John Sulewski for editorial assistance and thoughtful suggestions. These data were previously presented in poster format at the American Academy of Periodontology 2015 Annual Meeting, Orlando FL, November, 2015. Portions were presented in a poster session in "Lasers in Dentistry XXI," SPIE, San Francisco, CA, February, 2015. Supported in part by NIH-NIDCR SBIR DE016180 and NIH-NRSA DC008042 (D.M.H).

REFERENCES

1. Harris DM, Yessik M. Therapeutic ratio quantifies laser antisepsis: Ablation of Porphyromonas gingivalis with dental lasers. Lasers Surg Med 2004;35(3):206–213.
2. Ben Hatit Y, Blum R, Severin C, Maquin M, Jabro MH. The effects of a pulsed Nd:YAG laser on subgingival bacterial flora and on cementum: An in vivo study. J Clin Laser Med Surg 1996;14(3):137–143.
3. Cobb CM, McCawley TK, Killoy WJ. A preliminary study on the effects of the Nd:YAG laser on root surfaces and microflora in vivo. J Periodontol 1992;63(8):701–707.
4. Gutknecht N, Fischer J, Conrads G, Lampert F. Bactericidal effects of the Nd: YAG lasers in laser supported curettage. In: Wigdor HA, Featherstone JDB, Rechmann P, editors. Lasers in Dentistry III; 1997 Feb 8–9. San Jose, Calif. Proc. SPIE

2973. Bellingham, WA: SPIE—The International Society for Optical Engineereing; 1997. pp 221–226.
5. Gutknecht N, Van Betteray C, Ozturan S, Vanweersch L, Franzen R. Laser supported reduction of specific microorganisms in the periodontal pocket with the aid of an Er,Cr:YSGG laser: A pilot study. ScientificWorldJournal 2015; 2015:450258.
6. Neill ME, Mellonig JT. Clinical efficacy of the Nd:YAG laser for combination periodontitis therapy. Pract Periodontics Aesthet Dent 1997;9(6 Suppl):1–5.
7. Moritz A, Schoop U, Goharkhay K, Schauer P, Doertbudak O, Wernisch J, Sperr W. Treatment of periodontal pockets with a diode laser. Lasers Surg Med 1998;22(5):302–311.
8. Kamma JJ, Vasdekis BGS, Romanos GE. The effect of diode laser (980 nm) treatment on aggressive periodontitis: Evaluation of microbial and clinical parameters. Photomed Laser Surg 2009;27(1):11–19.
9. Derdilopoulou FV, Nonhoff J, Neumann K, Kielbassa AM. Microbiological findings after periodontal therapy using curettes, Er:YAG laser, sonic, and ultrasonic scalers. J Clin Periodontol 2007;34(7):588–598.
10. Kojima T, Shimada K, Iwasaki H, Ito K. Inhibitory effects of a super pulsed carbon dioxide laser at low energy density on periodontopathic bacteria and lipopolysaccharide *in vitro*. J Periodontal Res 2005;40(6):469–473.
11. Midda M, Renton-Harper P. Lasers in dentistry. Br Dent J 1991;170(9):343–346.
12. Meral G, Tasar F, Kocagöz S, Sener C. Factors affecting the antibacterial effects of Nd:YAG laser in vivo. Lasers Surg Med 2003;32(3):197–202.
13. Harris DM, Loomer PM. Ablation of Porphyromonas gingivalis *in vitro* with dental lasers. J Dent Res 2003;82(Spec. Issue A):abstract 0855.
14. Genco CA. Regulation of hemin and iron transport in Porphyromonas gingivalis. Adv Dent Res 1995;9(1):41–47.
15. Lamont RJ, Jenkinson HF. Life below the gum line: Pathogenic mechanisms of Porphyromonas gingivalis. Microbiol Mol Biol Rev 1998;62(4):1244–1263.
16. Bogen G, Slots J. Black-pigmented anaerobic rods in closed periapical lesions. Int Endod J 1999;32(3):204–210.
17. Leung KP, Subramaniam PS, Okamoto M, Fukushima H, Lai CH. The binding and utilization of hemoglobin by *Prevotella intermedia*. FEMS Microbiol Lett 1998;162(2):227–233.
18. Newkirk S, Slim L, Cobb CM. Laser assisted new attachment procedure (LANAP™): Strength of evidence. J West Soc Periodontol Periodontal Abstr 2015;63(1):3–7.
19. Mombelli A, Décaillet F. The characteristics of biofilms in peri-implant disease. J Clin Periodontol 2011;38(Suppl 11):203–213.
20. Leonhardt A, Renvert S, Dahlén G. Microbial findings at failing implants. Clin Oral Implants Res 1999;10(5):339–345.
21. Vieira Colombo AP, Magalhães CB, Hartenbach FA, Martins do Souto R, Maciel de Silva-Boghossian C. Periodontal-disease-associated biofilm: A reservoir for pathogens of medical importance. Microb Pathol 2015;pii: S0882-4010(15):00152–00157.
22. Canabarro A, Valle C, Farias MR, Santos FB, Lazera M, Wanke B. Association of subgingival colonization of Candida albicans and other yeasts with severity of chronic periodontitis. J Periodontal Res 2013;48(4):428–432.
23. Jacques SL. Ratio of entropy to enthalpy in thermal transitions in biological tissues. J Biomed Opt 2006;11(4): 041108-1–041108-7.
24. Harris DM, McDowell BA, Strisower J. Laser treatment for toenail fungus. In: Kollias N, Choi B, Zeng H, Malek RS, Wong BJ-F, Ilgner JFR, Gregory KW, Tearney GJ, Marcu L, Hirschberg H, Madsen SJ, editors. Photonic Therapeutics and Diagnostics V; 2009 Jan 24–26. SPIE—The International Society for Optical Engineering: San Jose, Calif. Proc. SPIE 7161. Bellingham, WA; 2009. pp 71610M-1–716107-7.
25. Giannelli M, Bani D, Viti C, Tani A, Lorenzini L, Zecchi-Orlandini S, Formigli L. Comparative evaluation of the effects of different photoablative laser irradiation protocols on the gingiva of periodontopathic patients. Photomed Laser Surg 2012;30(4):222–230.
26. Lamont RJ, Oda D, Persson RE, Persson GR. Interaction of *Porphyromonas gingivalis* with gingival epithelial cells maintained in culture. Oral Microbiol Immunol 1992;7(6): 364–367.
27. Deshpande RG, Khan M, Genco CA. Invasion strategies of the oral pathogen *Porphyromonas gingivalis*: Implications for cardiovascular disease. Invasion Metastasis 1998–1999; 18(2):57–69.
28. Duncan MJ, Nakao S, Skobe Z, Xie H. Interactions of *Porphyromonas gingivalis* with epithelial cells. Infect Immun 1993;61(5):2260–2265.
29. Reinisch L. Scatter-limited phototherapy: A model for laser treatment of skin. Lasers Surg Med 2002;30(5):381–388.
30. Reinisch L, Garrett GC, Courey M. A simplified laser treatment planning system: Proof of concept. Lasers Surg Med 2013;45(10):679–685.
31. Harris DM, Reinisch L, Jacques SJ, Darveau R. Selective destruction of periodontopathogens with dental lasers. Poster presented at: 101st Annual Meeting of the American Academy of Periodontology; 2015 Nov 14–17; Orlando, FL, Poster 59.
32. Harris DM, Reinisch L. Selective photoantisepsis. Lasers Surg Med 2016 (in press).
33. Jacques SL. Diffuse reflectance from a semiinfinite medium. May 17, 1999. http://omlc.ogi.edu/news/may99/rd/index.html. Accessed February 12, 2016.
34. Dorn BR, Leung K-P, Progulske-Fox A. Invasion of human oral epithelial cells by Prevotella intermedia. Infect Immun 1998;66(12):6054–6057.
35. Dorn BR, Dunn WA Jr, Progulske-Fox A. Invasion of coronary artery cells by periodontal pathogens. Infect Immun 1999;67(11):5792–5798.
36. *P. gingivalis* website: http://www.pgingivalis.org/ATCC33277(2).htm

APPENDIX

The deposition of laser energy in oral bacteria depends on the absorption coefficient, μ_a [cm^{-1}], of a single bacterium. However, it is difficult to make such measurements using standard spectrometers. A suspension of bacteria at sufficiently high concentration to provide significant absorption (about 10^9 cells/ml) yields a solution that is turbid. However, transmission of light through such a solution using a standard spectrometer is problematic. Attenuation due to scattering can be misinterpreted as attenuation due to absorption. In these pilot studies, the light scattering properties of the bacteria were measured by introducing the bacteria into a suspension of polystyrene microspheres in phosphate buffered saline. The suspension is milky in appearance due to the strong scattering properties of the microspheres. The addition of bacteria slightly colored the suspension. Reflectance measurements and subsequent analysis, described below, allow determination of the spectrum of the absorption coefficient from 400 to 1,100 nm of a single bacterium.

Absorption spectra of bacteria were measured by adding the bacterial suspension to the scattering solution of microspheres and measuring the change in reflectance relative to adding clear buffer. A 100% standard control was 0.6 ml of water added to the 1 ml of microspheres. Since absorption by the water was negligible, the diffuse reflectance

established the 100% reference point. A 0% standard control was 0.6 ml of India ink added to the 1 ml of microspheres. Since the ink's absorption was so strong, there was minimal diffuse reflectance and the signal was due primarily to stray specular reflectance that might enter the collection fiber. The bacteria, water and microspheres all absorbed light based on their absorption spectrums. We measure the attenuation caused by these absorbers in the diffuse reflection collected by the collection fiber. After normalizing for the response of the spectrometer, the spectrum of the light source and absorption by water and microspheres the remainder is the absorption due to the bacteria.

Oral bacteria were cultured on blood agar, then resuspended in phosphate buffer saline at a concentration of 10^9 cells/ml assayed by densitometry. Two species of oral pathogen were cultured: *Porphyromonas gingivalis* (*Pg*) and *Prevotella intermedia* (*Pi*). A total of 1 ml of each cell suspension was mixed with 2 ml of water and 1 ml of polystyrene microspheres (stock was 10% solids, 0.5 μm diameter). The resulting solutions were optically turbid with a slight discoloration due to the optical absorption properties of the bacteria. Each 4-ml mixture was placed into one well of a 12-well cell culture dish (Fig. 1, inset. Corning Inc Costar® 3526), which fully filled the well. In addition, a well with pure water was prepared to account for stray scattered light (called "BASE"), and a well with 2.5% solids microspheres was prepared as a standard with no added absorber (called "STD"). Each sample was illuminated with white light from a halogen lamp (Ocean Optics HL-2000) delivered by an optical fiber bundle from directly above the solution (Fig. 1). Spectral measurements of diffusely reflected light were acquired by an optical fiber viewing the sample at 45° off the vertical axis. In this way, most of the specular reflectance from the air/solution surface did not reach the collection fiber.

Figure 8 shows the raw spectral measurements, illustrating the magnitude of the STD signal and the BASE signal. The *Pg*, and *Pi* signals (called "sample") only slightly deviated from the STD signal. The reflectance (R) was calculated:

$$R = \frac{\text{sample} - \text{BASE}}{\text{STD} - \text{BASE}} \tag{1}$$

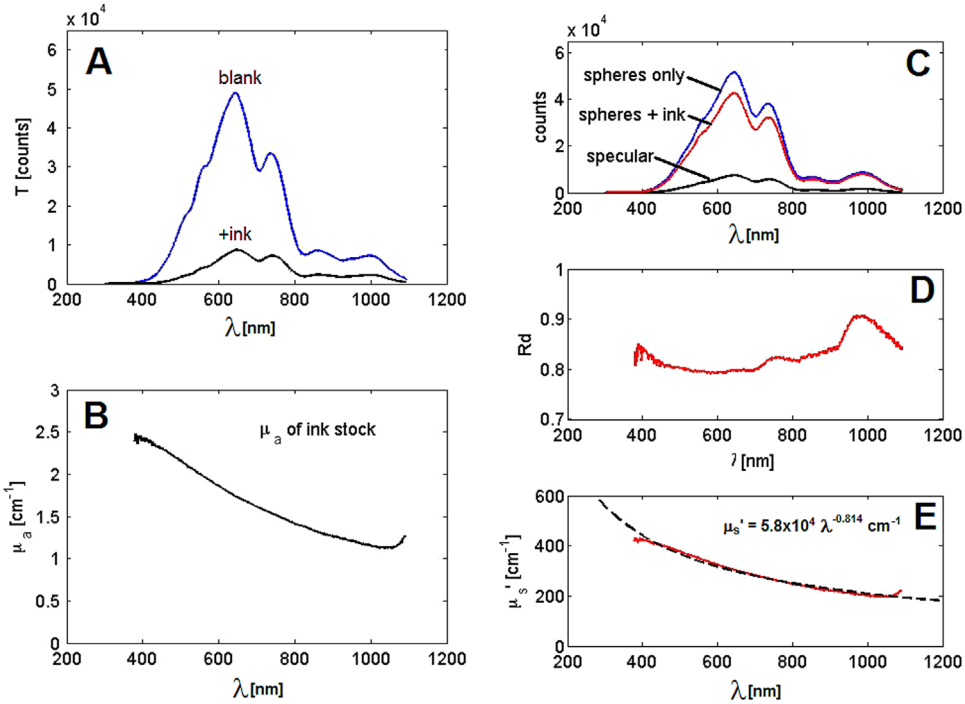

Fig. 8. Calibration experiment. Left: calibration of ink stock by transmission through a cuvette. (**A**) The raw transmission through a 1-cm cuvette. (**B**) The absorption coefficient $\mu_a = -\ln(T_{+\text{ink}}/T_{\text{blank}})/(1\,\text{cm})$. Right: calibration of scattering spectrum of sphere solution. (**C**) Raw reflectance spectra, including specular reflectance from 5% black ink solution (*R*sp), reflectance from 2.5% 0.500-mm-diameter polystyrene microspheres (*R*s), and reflectance from spheres with 0.098% ink (*R*i). (**D**) Reflectance of spheres plus ink: $R_d = (R_i - R_{sp})/(R_s - R_{sp})$. (**E**) The reduced scattering coefficient of the sphere solution, $\mu_s[\text{cm}^{-1}] = \mu_a \text{find}Np(R_d)$, where find$Np(R_d)$ is an algorithm that returns $Np = \mu_s'/\mu_a$ (Jacques [33]). The μ_s' of the sphere solution used to study the oral bacteria equaled $a\lambda^{-b}$, where λ is wavelength [nm], $a = 5.8 \times 104\,\text{cm}^{-1}$ and $b = 0.814$.

In separate experiments, the scattering properties of the microsphere solution were determined. Figure 8 shows the results of the cuvette experiments for calibration of the India ink absorption properties and the microsphere scattering properties. First, the absorption properties of an India ink solution were determined by transmission through a cuvette containing either a blank or the 0.1% ink solution (Fig. 8A).
Measurements of reflectance from the microsphere solution (R_s), the microsphere solution with 0.025% ink added (0.1% ink diluted 1/4 ml) (R_i), and the specular reflectance from the surface of a very black 5% ink solution (R_{sp}) were acquired (Fig. 8C). Then the diffuse reflectance (R_d) of the solution was calculated (Fig. 8D):

$$R_d = \frac{R_i - R_{\mathrm{sp}}}{R_s - R_{\mathrm{sp}}} \tag{2}$$

The total diffuse reflectance, R_d, from a semi-infinite medium is a unique function of the ratio $N_p = \mu_s'/\mu_a$. The reduced scattering coefficient, μ_s', is a lumped property incorporating the scattering coefficient μ_s and the anisotropy. An algorithm find$N_p(R_d)$ [33] was based on Adding Doubling Method calculations and verified by Monte Carlo simulations. find$N_p(R_d)$ returns the value N_p. Hence,

$$\mu_s' = \mu_a \ \mathrm{find}Np(R_d) \tag{3}$$

The value of μ_s' [cm^{-1}] *versus* wavelength, λ [nm], was deduced from the experimental data, and fit with the following expression (Fig. 9E):

$$\mu_s' = a\lambda^{-b} = 5.7 \times 10^4 \lambda^{-0.814} \tag{4}$$

Once the microsphere solution was calibrated, the absorption properties of the bacteria solutions were determined by using Equations (2) and (3). The absorption spectrum of a single bacterial cell, calculated as:

$$\mu_a = \frac{\mu_s' \ \mathrm{find}Np(R_d)}{4 \ 10^9 \ V_{\mathrm{cell}}} \tag{5}$$

where R_d was calculated using Equation (2), and V_{cell} is the volume of a cell with a spherical shape with 1-μm diameter.

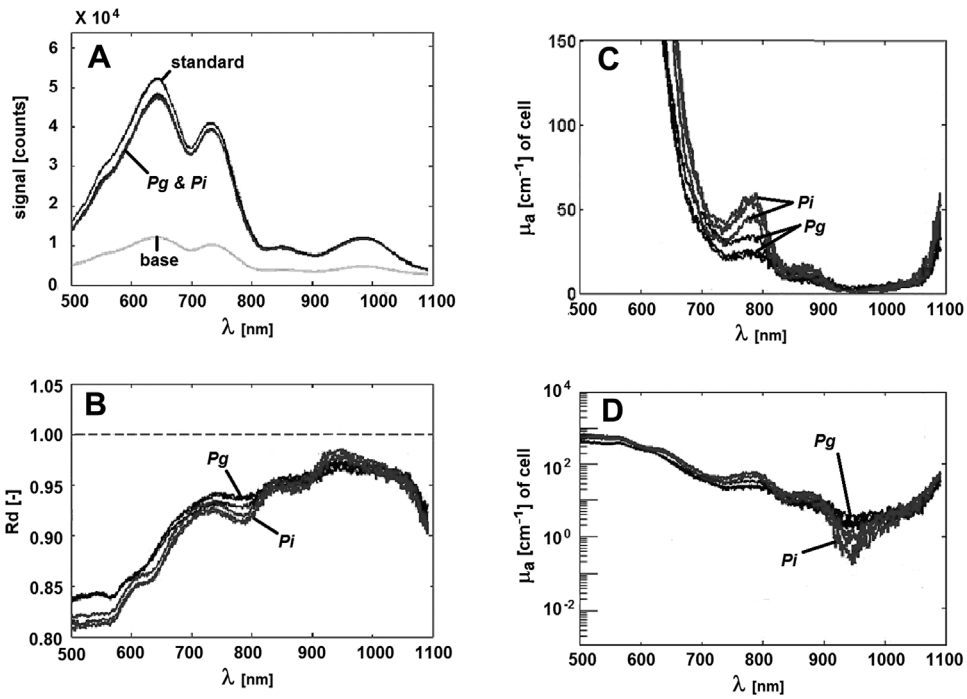

Fig. 9. Experiments with oral bacteria. (**A**) Experimental results showing counts for the two bacterial solutions (*Pg*, *Pi*,), the polystyrene microsphere solution without bacteria (standard), and the specular reflectance from a clear water solution (base). (**B**) The calculated reflectance of the bacterial solutions. Right: The absorption coefficient of a 1-μm-diameter spherical bacterium based on the cell number density of 109 cells/ml. Linear scale (**C**) and log scale (**D**).

The factor 4 corrects for the 1/4 dilution of the original bacterial solution containing 10^9 cells/ml. The factor 10^9 corrects for the number density of cells. This size and shape assumption provides an estimate for this calculation of the absorption coefficient, μ_a, of a cell. *Pg* and *Pi* are ideal candidates for mathematical modeling. Numerous published microscopic images confirm that a 1-μm sphere is a close approximation of the actual shape and size of these bacteria (e.g., Dorn, 1998, Fig. 2 [26]; Dorn, 1999, Figs. 1–3 [34]; Lamont, Figs. 4 and 5 [35]; *P. gingivalis* website [36]).

Figure 9 shows the experimental measurements of the control and bacterial solutions (Fig. 9A), and the calculated diffuse reflectance R_d (Fig. 9B). On the right is the calculated μ_a spectrum for one cell on both linear (Fig. 9C) and logarithmic (Figs. 2 and 9D) scales.